

II. MODEL AND METHOD

This Section presents the spin-motion coupled Ising model used to describe experiments of Rydberg atoms in optical lattices or microtrap arrays [Sec. II A] and the dTWA methods used to calculate the dynamics [Sec. II B].

A. Spin-motion Coupled Ising Model

The experimental system we consider is an array of atoms in a 2D square lattice at unit filling driven by a laser that couples ground state atoms $|g\rangle = |\downarrow\rangle$ to a low-lying Rydberg state $|r\rangle = |\uparrow\rangle$, with Rabi frequency Ω and detuning Δ , as shown in Fig. 1. In the spin language, the Ω and Δ give transverse and longitudinal fields, respectively. There is an attractive van der Waals (vdW) interaction when two atoms are in the Rydberg state, giving rise to an Ising coupling between spins that is C_6/R^6 where R is the distance between spins. The nearest-neighbor terms dominate for the parameters in Ref. [18], so we neglect longer-ranged interactions.

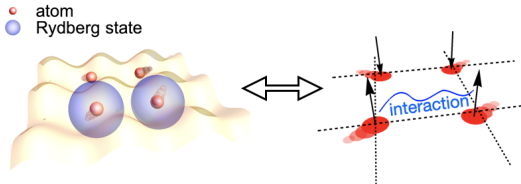


FIG. 1. (color online) A 2D optical lattice of atoms with two internal states coupled by a laser realizes a transverse-field Ising model with $|\downarrow\rangle$ and $|\uparrow\rangle$ given by the ground state $|g\rangle$ and a Rydberg state $|r\rangle$, respectively. Two atoms interact only if both are in $|\uparrow\rangle$, as described by Eq. (1). Spins (atoms) are allowed to move, as indicated by the pale red trails.

Atoms move due to their initial velocities and the vdW interaction among those in the Rydberg state, and the Ising model must be extended to capture the kinetic energy and the optical forces on the atoms. We assume atom i is trapped by a 3D harmonic oscillator centered at lattice site i , which is valid in a deep lattice as long as the atoms are not too far displaced from their equilibrium position \vec{R}_i . Then the appropriate Hamiltonian is

$$\begin{aligned}
 H = & \frac{\hbar}{2} \sum_i (\Omega \sigma_i^x - \Delta \sigma_i^z) \\
 & - \frac{\hbar J}{8} \sum_{\langle i,j \rangle} \left(\frac{a_l}{r_{ij}} \right)^6 (\sigma_i^z + 1)(\sigma_j^z + 1) \\
 & + \sum_{i,\alpha} \frac{p_i^{\alpha 2}}{2m} + \sum_i \hbar V_0 \frac{\pi^2}{2a_l^2} \tilde{r}_i^2 (1 - \sigma_i^z), \quad (1)
 \end{aligned}$$

where a_l is the lattice constant, $J = |C_6|/a_l^6$ is the nearest-neighbor interaction strength, p_i^α is atom i 's mo-

mentum in direction α ($\alpha = x, y, z$), σ_i^α is the Pauli matrix for atom i , r_{ij} is the distance between two atoms i and j that are located at \vec{r}_i and \vec{r}_j , and \tilde{r}_i is the magnitude of the displacement $\vec{\tilde{r}}_i = \vec{r}_i - \vec{R}_i$ of atom i from the center of lattice site. We neglect the trap potential on atoms in the Rydberg state, as it is much smaller than the trap on ground-state atoms as well as negligible compared to the Rydberg-Rydberg interaction.

Most of our concrete calculations are for Lithium-6 atoms in an optical lattice in the experimental configuration of Ref. [18], but the broad results apply more generally, for example to other atoms and microtrap potentials, which are discussed in Sec. IV. When considering the experiments in Ref. [18], we take the lattice depth to be $V_0 = 55E_R/\hbar$, where $E_R = \pi^2 \hbar^2 / 2ma_l^2$ is the recoil energy and $a_l = 1024/\sqrt{2}\text{nm}$, and $C_6/a_l^6 = -2\pi \times 6.0\text{MHz}$, the result from experimental fitting in Ref. [18]. Throughout our calculation, we neglect the single-particle decoherence unless otherwise specified. To measure how the system deviates from product states, we focus on the connected spin-spin correlation

$$C(i, j) = \langle \sigma_i^z \sigma_j^z \rangle - \langle \sigma_i^z \rangle \langle \sigma_j^z \rangle. \quad (2)$$

B. Discrete Truncated Wigner Approximation

In the area of quantum spin dynamics, the truncated Wigner approximation (TWA) methods are widely used, especially for quenches and when timescales are not too long. These methods are controlled approximations when the correlations between particles are small or the system is semiclassical [31]. Additionally, the dTWA method [27, 32–34], which maps the spin degree of freedom to a discrete phase space, can also preserve oscillating features [29, 30] and capture correlations [28] on moderate timescales; often, it outperforms the continuous TWA in 1D spin chains [34]. Recent studies [29, 35–37] compare results from dTWA to exact results, higher order dTWA calculations, or Rydberg atom experiments and reveal that dTWA methods in 2D spin systems can be accurate for timescales of $Jt \simeq 2$, comparable to the largest timescales studied in this paper. TWA methods approximate quantum dynamics by classical equations of motion (EoM) propagated from the exact initial state's Wigner distribution (quasiprobability) [31]. The EoM's are derived from the Hamiltonian (1) and shown in Appendix A. We use the same random seed for calculations with different physical parameters.

For atoms in a harmonic trap with frequency ω at temperature T , the Wigner distribution is

$$W(x, p) = 2 \tanh \left(\frac{\hbar \omega}{2k_B T} \right) \exp \left(- \frac{(x/\ell)^2 + (p\ell/\hbar)^2}{\coth \left(\frac{\hbar \omega}{2k_B T} \right)} \right), \quad (3)$$

where $\ell = \sqrt{\hbar/m\omega}$ is the harmonic oscillator length. $T = 0$ yields the ground-state Wigner distribution. For the spins, dTWA represents the spin- $\frac{1}{2}$ observables as

points in a discrete phase space [27, 38], which we take to be the eight points $\vec{S}_u \in \frac{1}{2}(\pm 1, \pm 1, \pm 1)$. Ref. [34] has shown that this choice of basis performs better than other choices in a broad range of scenarios [32]. When the initial spins are aligned in the $|\downarrow\rangle$ state, the quasiprobability $W(\vec{S}_u)$ is $\frac{1}{4}$ for the four points $\frac{1}{2}(\pm 1, \pm 1, -1)$ and 0 for the other four.

Our dTWA and exact diagonalization (ED) calculations are for a 4×4 lattice with periodic boundary condition. We have calculated results for a 6×6 system with dTWA and they agree well with the 4×4 results. For example, for the long-time quench results discussed in Sec. III A 2, the differences of the correlation between two system sizes are always less (usually much less) than 6% for the range of Δ 's plotted, and for shorter times these differences are smaller. For both ED dynamics and solving the classical EoM, we use fourth-order Runge–Kutta with a timestep of 1ns for the ideal Ising model and 0.5ns for the motional model. The results are well-converged: for example, decreasing the integration timestep by a factor of two for the ideal Ising long-time quench discussed in Sec. III A 2 changes all results by less than 2%. Statistical errors are small and indicated in the figures.

III. RESULTS: QUENCH AND RAMP DYNAMICS

A. Sudden Quench

Motivated by Ref. [18], the first scenario we study is quench dynamics of the Rydberg atoms in an optical lattice. Specifically, the lattice is initially filled with exactly one atom per site, which is in its electronic ground state and in its motional ground state. (Sec. IV considers finite-temperature motional states as well.) After an instantaneous turn-on of Ω , the system evolves under Eq. (1). We study two quenches: “short-time quenches” with $\Omega t < 1$ (Sec. III A 1) and “long-time quenches” with $\Omega t > 1$ (Sec. III A 2). For each quench, we calculate the spin correlations $C(i, j)$ as a function of detuning Δ .

1. Short-time Quench

Figures 2(a) and (b) show that the effect of motion is small but observable for the short-time quench ($\Omega t = 0.5$) dynamics. In these calculations, we use the Rabi frequency ($\Omega = 2\pi \times 4.1\text{MHz}$) and duration ($t = 61\text{ns}$) from the experiments in Ref. [18]. We compare three versions of the spin model: (i) the ideal Ising model with all spins sitting at the center of individual lattice sites; (ii) the frozen model, where each atom has a finite distribution of locations initially, but does not move during the spin dynamics; (iii) the full motion model, where each atom has both an initial distribution of locations and momenta, and it is allowed to move according to interactions with other atoms and the lattice.

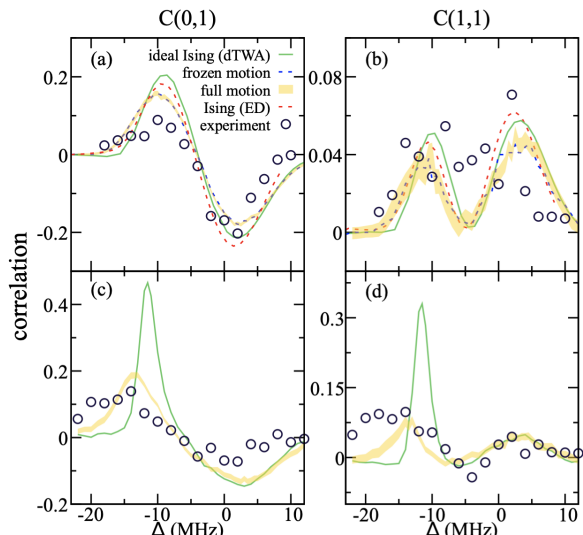


FIG. 2. (color online) Spin correlations at short duration (top row, $\Omega t = 0.5$, 61ns, 5,000 dTWA trajectories) and at long duration (bottom row, $\Omega t = 2.97$, 280ns, 2,000 dTWA trajectories) after a sudden quench with different Δ values. The circles are experimental data from Ref. [18] and the curves are theory calculations described in the text. The shaded region indicates ± 1 standard error of the mean, and to avoid clutter are shown only on the full motion results, which are the results with the largest statistical errors.

Figures 2(a) and (b) shows that the motion modifies the correlations even on these short timescales, as seen by comparing the ideal Ising and the full motion model. However, for this timescale, the dominant contribution comes from initial spread of atom positions rather than atom motion during the quench, evidenced by the close agreement between the full-motion and frozen-motion results.

Figure 2 also shows results obtained by 4×4 ED of the pure spin system. Comparing this and the dTWA method confirms that the latter is an accurate approximation in the situations shown.

2. Long-time Quench

Figures 2(c) and (d) show that atom motion significantly suppresses the growth of correlations in the long-time quench dynamics with $\Omega t = 2.97$, using the corresponding experimental $\Omega = 2\pi \times 5.4\text{MHz}$ and $t = 280\text{ns}$.

The simulations with atom motion qualitatively reproduce the experimental long-time quench results. Upon incorporating the initial state effects and motion during the dynamics (the full motion model), the height of the correlation peaks is dramatically reduced, in agreement with the experimental values. The atom motion also broadens and shifts the peaks. We have found that the frozen motion model [omitted for clarity in Fig. 2(c) and (d)] deviates strongly from the full motion results.

Comparing short and long duration quenches demon-

strates that the effects of motion increase over time. The evolution of correlations in both ideal Ising and full motion models, as shown in Appendix B, confirms that the effect of motion accumulates over time and shows up after $t = 50\text{ns}$ in this experimental setting, independent of the detuning. A drastic increasing of kinetic energy, specifically in the transverse direction, is also observed in Appendix B.

B. Slow Quench with Detuning Ramp

Again motivated by Ref. [18], the second scenario we study is the dynamics as the longitudinal field Δ is slowly swept from far off resonance to the final detuning. For sufficiently slow ramps, coherent evolution, and no motional coupling, this would result in adiabatic preparation of the Ising ground state. The dynamics has two stages, as in the experiment Ref. [18]. Initially, all the atoms are prepared in the ground state under a laser field with Rabi frequency Ω_i and large laser detuning $\Delta_i \gg J$. The first stage of the ramping process is that the Δ decreases to a preset value Δ_f with a given ramp rate $\dot{\Delta}$ while Ω is constant. The second stage is a linear turn-off of the Ω with rate $\dot{\Omega}$ while Δ holds constant. We focus on the experimental parameter values: $J = 2\pi \times 6\text{MHz}$, $\Omega_i = 0.9J$, $\Delta_i = 3.3J$, and $\dot{\Omega} = 0.24J^2$, and we take the single-body decoherence times, specifically the lifetime and dephasing time, to be $T_1 = 20\mu\text{s}$ and $T_2 = 0.5\mu\text{s}$, respectively. The single-body decoherence is incorporated into the calculations as described in Appendix A.

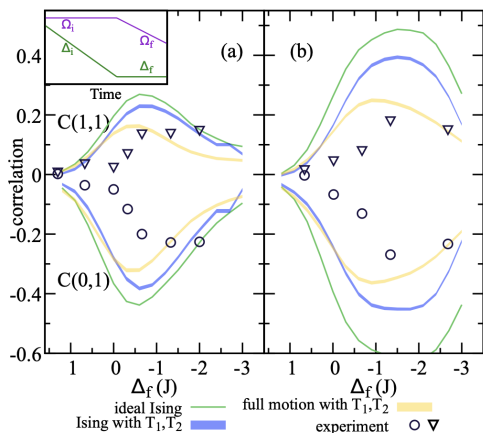


FIG. 3. (color online) Ramp results varying Δ_f . (a) $\dot{\Delta} = -1.42J^2$. The fields Ω and Δ vary over time in two stages, as shown in the inset and described in the text. (b) $\dot{\Delta} = -0.70J^2$. The solid curves are the ideal Ising results. The two shaded regions, which indicate ± 1 standard error of the mean, are Ising and full motion model results, each with single-body T_1 and T_2 decoherence. Note that the horizontal axis is reversed.

Figure 3 shows results for two ramp rates $\dot{\Delta}$, in order to compare motional effects at different timescales. For the shortest duration ramps [Fig. 3(a) at positive Δ_f], the

single-atom noise can play a more important role than the atom motion. However, the effect of motion rapidly appears and exceeds the single-atom noise, as seen in Fig. 3(a) for negative Δ_f and Fig. 3(b) for nearly all Δ_f . In Fig. 3(b), as the sweeping is slower (with smaller $\dot{\Delta}$), the process will be closer to an adiabatic process and build up a higher correlation peak. However, as this process takes longer time, the effect of the atom motion is even larger.

The dTWA simulation supports Ref. [18]’s conjecture that atom motion is a significant source of decoherence in the detuning ramp results. Even though there are some differences between simulation and experiments that are possibly caused either by the limit of the dTWA method or the simplification in the model, the numerical results agree roughly with the experimentally-observed correlations as a function of detuning [18], and give a peak magnitude quantitatively consistent with the experiment. As the atom motion is introduced to the model without any fitting, our results give a reasonable explanation of Ref. [18] two-body interaction noise.

IV. EFFECT OF MOTION IN OPTICAL TWEEZERS

The results above have shown the importance of motion in recent optical lattice experiments, raising the question of what role atom motion plays more generally in ongoing experiments with optical lattices and microtraps, another important technique to realize spin models with Rydberg atoms [11, 13]. In this section, we answer two relevant questions: First, what are possible ways to mitigate the motional effects in optical lattices? Second, what is the effect of atom motion in optical tweezer experiments?

A. Suppressing motional decoherence

Intuitively, the effect of motion will be smaller in deeper lattice or with heavier atoms. Our calculations show that replacing lithium atoms with rubidium atoms or increasing the lattice depth can help to reduce, but not eliminate, the motional effects, as shown in Fig. 4. In dynamics similar to the long-time quench in Sec. III A 2 ($\Omega t = 2.97$), using heavier atoms (Rb) or applying a deeper trap ($V = 10V_0$) increases the height of correlation peaks and is closer to the ideal Ising result. However, the peak remains much lower than in the ideal Ising dynamics and shifts noticeably. Because these techniques only partially alleviate the motional decoherence, atom motion will be important to consider when designing future experiments.

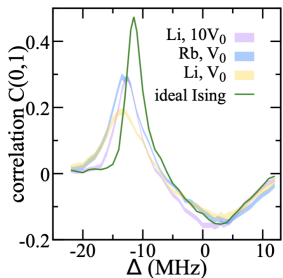


FIG. 4. (color online) Long time ($\Omega t = 2.97$) quench when Rb atoms are used or the depth of the lattice increases to $10V_0$, where V_0 is the lattice depth applied in Sec. III. These two results are plotted in comparison to the ideal Ising and full motion results of the original setting. The shaded region indicates ± 1 standard error of the mean.

B. Motional decoherence in microtraps

Although the programmability of microtraps leads to a diversity of geometries, the effect of motion is generally expected to be smaller in microtraps than lattices, due to the microtraps' deeper wells. To evaluate these effects, we simulate the sudden quench dynamics with atom motion in microtraps in recently-used experimental conditions with ^{87}Rb [11, 39]. The parameters include $a_l = 10\mu\text{m}$, $C_6 = \pm 2\pi \times 1.95\text{MHz}a_l^6$, $\Omega = 2\pi \times 1.95\text{MHz}$, and a radial (longitudinal) harmonic oscillator frequency near the trap center of 100kHz (20kHz).

The quench duration is 760ns , which gives the same Ωt value as the long-time quench discussed in Sec. III A. The results are shown in Fig. 5, along with the dTWA results of the ideal Ising model for comparison. It should be noted that the atoms in microtraps are not fully cooled down after the preparation of the experiment. Thus, the initial conditions [Eq. (3)] correspond to the atoms' temperature in the magneto-optical trap, which is $25\mu\text{K}$ [39].

Figure 5(a) shows that in microtraps with repulsive dipole-dipole interactions, a common case in experiments [11, 13], the motional effects are fairly small in the timescale we considered. After the sudden quench, the full motion model's peak in $C(0,1)$ has the same height as in the ideal Ising model, but with a slightly shifted position.

An important point is that in ongoing microtrap experiments, Jt is 10 times larger than we consider here [11]. We have performed dTWA calculations for such timescales, seeing a much larger motional effect. This is not included in the figures because the strong quantum fluctuations and correlations at the longer times make our dTWA method questionable. Nevertheless, our results here suggest that the effect of motional decoherence should already be detectable at much shorter times, and, as discussed in Sec. III A 2, it is reasonable to expect an increase in this motional effect at longer times.

Finally, we note that the sign of the interaction changes the motional effects as shown in Fig. 5(b). The effect of motion for repulsive interactions is less significant than

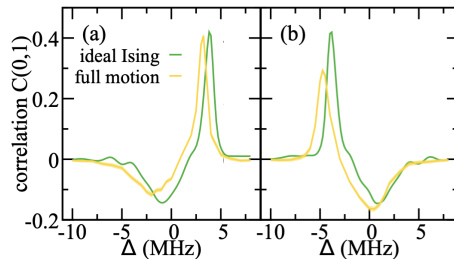


FIG. 5. (color online) Sudden quench results for Rydberg-atom lattice based on Rb atoms trapped in microtraps, under different detuning values. The quench time is 760ns ($\Omega t = 2.97$). (a) $C(0,1)$ with repulsive vdW interaction; (b) $C(0,1)$ with attractive interaction. The shaded region indicates ± 1 standard error of the mean.

that for attractive interactions. The $C(0,1)$ in the attractive Rydberg-atom lattice [Fig. 5(b)] shows a suppression of peak height by the atom motion, which is not observed in the repulsive model in Fig. 5(a). The atom motion in the attractive model also shifts the peak position.

V. CONCLUSION

In summary, we show that atom motion affects the evolution of correlations in Rydberg-atom lattices, which explains the discrepancy between coherent results and recent experimental observations. For example, the results indicate that atom motion suppresses magnetic correlations, sometimes by a large amount.

We also suggest possible ways to relieve the effect of atom motion including using heavier atoms, deeper lattices, or repulsive Rydberg-Rydberg interactions. All of these methods, which are usable in current experiments, can reduce, but not eliminate, the motional decoherence on the timescales we have considered. As the Rydberg atom platforms become a major toolbox in quantum simulation and quantum computation, knowing the existence of motional decoherence, especially its magnitude in different timescales, is helpful both to design experiments and analyze results. Another route worth investigating to suppress motional decoherence is to use ultrafast dynamics, as in recent experiments in Refs. [3, 40, 41]. Here, the short timescales minimize the thermal motion. If interaction-induced motion also remains slow compared to the ultrafast timescales, this platform may offer a route to simulating long-time spin dynamics with minimal motional effects.

Interesting future questions include how the motional dynamics interplays with other sources of noise including disorder in the lattice [11], blackbody-induced broadening [42, 43] or transitions [44], and motion-facilitated excitation [21, 43]. We have noticed that some quantitative differences remain between the dTWA simulation and experiments. To understand this, one may look to improve the motional Rydberg-atom lattice model to include effects of longer-range interaction [18], shapes of Rydberg-

Rydberg interaction [20], and to extend the numerical methods to capture the strong quantum fluctuations that occur at larger timescales [30, 45].

ACKNOWLEDGMENTS

We thank Fei Gao for conversations about related calculations. We acknowledge support by the Welch Foun-

dation Grant No. C1872, the Office of Naval Research Grant No. N00014-20-1-2695, and the National Science Foundation Grant No. PHY1848304. K.H.'s contribution benefited from discussions at the KITP, which was supported in part by the National Science Foundation under Grant No. NSF PHY-1748958.

-
- [1] J. Zeiher, R. Van Bijnen, P. Schauß, S. Hild, J.-y. Choi, T. Pohl, I. Bloch, and C. Gross, Many-body interferometry of a Rydberg-dressed spin lattice, *Nat. Phys.* **12**, 1095 (2016).
- [2] E. Guardado-Sanchez, B. Spar, P. Schauss, R. Belyansky, J. T. Young, P. Bienias, A. V. Gorshkov, T. Iadecola, and W. S. Bakr, Quench dynamics of a Fermi gas with strong long-range interactions, *Energy* **10**, 1 (2020).
- [3] V. Bharti, S. Sugawa, M. Mizoguchi, M. Kunimi, Y. Zhang, S. de Léséleuc, T. Tomita, T. Franz, M. Weidemüller, and K. Ohmori, Ultrafast many-body dynamics in an ultracold Rydberg-excited atomic Mott insulator, arXiv preprint arXiv:2201.09590 (2022).
- [4] H. Labuhn, D. Barredo, S. Ravets, S. De Léséleuc, T. Macrì, T. Lahaye, and A. Browaeys, Tunable two-dimensional arrays of single Rydberg atoms for realizing quantum Ising models, *Nature* **534**, 667 (2016).
- [5] D. O. de Mello, D. Schäffner, J. Werkmann, T. Preuschoff, L. Kohfahl, M. Schlosser, and G. Birkel, Defect-free assembly of 2D clusters of more than 100 single-atom quantum systems, *Phys. Rev. Lett.* **122**, 203601 (2019).
- [6] F. M. Gambetta, W. Li, F. Schmidt-Kaler, and I. Lesanovsky, Engineering nonbinary Rydberg interactions via phonons in an optical lattice, *Phys. Rev. Lett.* **124**, 043402 (2020).
- [7] H. Bernien, S. Schwartz, A. Keesling, H. Levine, A. Omran, H. Pichler, S. Choi, A. S. Zibrov, M. Endres, M. Greiner, *et al.*, Probing many-body dynamics on a 51-atom quantum simulator, *Nature* **551**, 579 (2017).
- [8] H. Kim, Y. Park, K. Kim, H.-S. Sim, and J. Ahn, Detailed balance of thermalization dynamics in Rydberg-atom quantum simulators, *Phys. Rev. Lett.* **120**, 180502 (2018).
- [9] V. Lienhard, S. de Léséleuc, D. Barredo, T. Lahaye, A. Browaeys, M. Schuler, L.-P. Henry, and A. M. Läuchli, Observing the space-and time-dependent growth of correlations in dynamically tuned synthetic Ising models with antiferromagnetic interactions, *Phys. Rev. X* **8**, 021070 (2018).
- [10] S. De Léséleuc, S. Weber, V. Lienhard, D. Barredo, H. P. Büchler, T. Lahaye, and A. Browaeys, Accurate mapping of multilevel Rydberg atoms on interacting spin-1/2 particles for the quantum simulation of Ising models, *Phys. Rev. Lett.* **120**, 113602 (2018).
- [11] P. Scholl, M. Schuler, H. J. Williams, A. A. Eberharter, D. Barredo, K.-N. Schymik, V. Lienhard, L.-P. Henry, T. C. Lang, T. Lahaye, *et al.*, Quantum simulation of 2D antiferromagnets with hundreds of Rydberg atoms, *Nature* **595**, 233 (2021).
- [12] A. Browaeys and T. Lahaye, Many-body physics with individually controlled Rydberg atoms, *Nat. Phys.* **16**, 132 (2020).
- [13] S. Ebadi, T. T. Wang, H. Levine, A. Keesling, G. Semeghini, A. Omran, D. Bluvstein, R. Samajdar, H. Pichler, W. W. Ho, *et al.*, Quantum phases of matter on a 256-atom programmable quantum simulator, *Nature* **595**, 227 (2021).
- [14] G. Semeghini, H. Levine, A. Keesling, S. Ebadi, T. T. Wang, D. Bluvstein, R. Verresen, H. Pichler, M. Kalinowski, R. Samajdar, A. Omran, S. Sachdev, A. Vishwanath, M. Greiner, V. Vuletić, and M. D. Lukin, Probing topological spin liquids on a programmable quantum simulator, *Science* **374**, 1242 (2021).
- [15] Y. Song, M. Kim, H. Hwang, W. Lee, and J. Ahn, Quantum simulation of Cayley-tree Ising Hamiltonians with three-dimensional Rydberg atoms, *Phys. Rev. Res.* **3**, 013286 (2021).
- [16] A. Dauphin, M. Müller, and M. A. Martin-Delgado, Quantum simulation of a topological Mott insulator with Rydberg atoms in a Lieb lattice, *Phys. Rev. A* **93**, 043611 (2016).
- [17] F. Grusdt, M. Kánasz-Nagy, A. Bohrdt, C. S. Chiu, G. Ji, M. Greiner, D. Greif, and E. Demler, Parton theory of magnetic polarons: Mesonic resonances and signatures in dynamics, *Phys. Rev. X* **8**, 011046 (2018).
- [18] E. Guardado-Sanchez, P. T. Brown, D. Mitra, T. Devakul, D. A. Huse, P. Schauß, and W. S. Bakr, Probing the quench dynamics of antiferromagnetic correlations in a 2D quantum Ising spin system, *Phys. Rev. X* **8**, 021069 (2018).
- [19] W. Li, C. Ates, and I. Lesanovsky, Nonadiabatic motional effects and dissipative blockade for Rydberg atoms excited from optical lattices or microtraps, *Phys. Rev. Lett.* **110**, 213005 (2013).
- [20] T. Macrì and T. Pohl, Rydberg dressing of atoms in optical lattices, *Phys. Rev. A* **89**, 011402 (2014).
- [21] L. Festa, N. Lorenz, L.-M. Steinert, Z. Chen, P. Osterholz, R. Eberhard, and C. Gross, Blackbody-radiation-induced facilitated excitation of Rydberg atoms in optical tweezers, *Phys. Rev. A* **105**, 013109 (2022).
- [22] Y. Dudin and A. Kuzmich, Strongly interacting Rydberg excitations of a cold atomic gas, *Science* **336**, 887 (2012).
- [23] S. Baur, D. Tiarks, G. Rempe, and S. Dürr, Single-photon switch based on Rydberg blockade, *Phys. Rev. Lett.* **112**, 073901 (2014).
- [24] M. M. Müller, M. Murphy, S. Montangero, T. Calarco, P. Grangier, and A. Browaeys, Implementation of an ex-

- perimentally feasible controlled-phase gate on two blockaded Rydberg atoms, *Phys. Rev. A* **89**, 032334 (2014).
- [25] J. Han, T. Vogt, and W. Li, Spectral shift and dephasing of electromagnetically induced transparency in an interacting Rydberg gas, *Phys. Rev. A* **94**, 043806 (2016).
- [26] M. Marcuzzi, J. Minář, D. Barredo, S. De Léséleuc, H. Labuhn, T. Lahaye, A. Browaeys, E. Levi, and I. Lesanovsky, Facilitation dynamics and localization phenomena in Rydberg lattice gases with position disorder, *Phys. Rev. Lett.* **118**, 063606 (2017).
- [27] J. Schachenmayer, A. Pikovski, and A. M. Rey, Many-body quantum spin dynamics with Monte Carlo trajectories on a discrete phase space, *Phys. Rev. X* **5**, 011022 (2015).
- [28] R. Khassseh, A. Russomanno, M. Schmitt, M. Heyl, and R. Fazio, Discrete truncated Wigner approach to dynamical phase transitions in Ising models after a quantum quench, *Phys. Rev. B* **102**, 014303 (2020).
- [29] M. Kunimi, K. Nagao, S. Goto, and I. Danshita, Performance evaluation of the discrete truncated Wigner approximation for quench dynamics of quantum spin systems with long-range interactions, *Phys. Rev. Res.* **3**, 013060 (2021).
- [30] S. Czischek, M. Gärttner, M. Oberthaler, M. Kastner, and T. Gasenzer, Quenches near criticality of the quantum Ising chain—power and limitations of the discrete truncated Wigner approximation, *Quantum Sci. Technol.* **4**, 014006 (2018).
- [31] A. Polkovnikov, Phase space representation of quantum dynamics, *Ann. Phys.* **325**, 1790 (2010).
- [32] L. Pucci, A. Roy, and M. Kastner, Simulation of quantum spin dynamics by phase space sampling of Bogoliubov-Born-Green-Kirkwood-Yvon trajectories, *Phys. Rev. B* **93**, 174302 (2016).
- [33] O. Acevedo, A. Safavi-Naini, J. Schachenmayer, M. Wall, R. Nandkishore, and A. Rey, Exploring many-body localization and thermalization using semiclassical methods, *Phys. Rev. A* **96**, 033604 (2017).
- [34] B. Sundar, K. C. Wang, and K. R. A. Hazzard, Analysis of continuous and discrete Wigner approximations for spin dynamics, *Phys. Rev. A* **99**, 043627 (2019).
- [35] J. Schachenmayer, A. Pikovski, and A. M. Rey, Dynamics of correlations in two-dimensional quantum spin models with long-range interactions: a phase-space Monte-Carlo study, *New J. Phys.* **17**, 065009 (2015).
- [36] A. Signoles, T. Franz, R. F. Alves, M. Gärttner, S. Whitlock, G. Zürn, and M. Weidemüller, Glassy dynamics in a disordered Heisenberg quantum spin system, *Phys. Rev. X* **11**, 011011 (2021).
- [37] A. Schuckert, I. Lovas, and M. Knap, Nonlocal emergent hydrodynamics in a long-range quantum spin system, *Phys. Rev. B* **101**, 020416 (2020).
- [38] W. K. Wootters, A Wigner-function formulation of finite-state quantum mechanics, *Ann. Phys.* **176**, 1 (1987).
- [39] D. Barredo, V. Lienhard, S. De Léséleuc, T. Lahaye, and A. Browaeys, Synthetic three-dimensional atomic structures assembled atom by atom, *Nature* **561**, 79 (2018).
- [40] N. Takei, C. Sommer, C. Genes, G. Pupillo, H. Goto, K. Koyasu, H. Chiba, M. Weidemüller, and K. Ohmori, Direct observation of ultrafast many-body electron dynamics in an ultracold Rydberg gas, *Nat. Commun.* **7**, 1 (2016).
- [41] C. Sommer, G. Pupillo, N. Takei, S. Takeda, A. Tanaka, K. Ohmori, and C. Genes, Time-domain Ramsey interferometry with interacting Rydberg atoms, *Phys. Rev. A* **94**, 053607 (2016).
- [42] E. A. Goldschmidt, T. Boulier, R. C. Brown, S. B. Koller, J. T. Young, A. V. Gorshkov, S. Rolston, and J. V. Porto, Anomalous broadening in driven dissipative Rydberg systems, *Phys. Rev. Lett.* **116**, 113001 (2016).
- [43] T. Boulier, E. Magnan, C. Bracamontes, J. Maslek, E. Goldschmidt, J. Young, A. V. Gorshkov, S. Rolston, and J. V. Porto, Spontaneous avalanche dephasing in large Rydberg ensembles, *Phys. Rev. A* **96**, 053409 (2017).
- [44] J. Aman, B. J. DeSalvo, F. Dunning, T. Killian, S. Yoshida, and J. Burgdörfer, Trap losses induced by near-resonant Rydberg dressing of cold atomic gases, *Phys. Rev. A* **93**, 043425 (2016).
- [45] J. Wurtz, A. Polkovnikov, and D. Sels, Cluster truncated Wigner approximation in strongly interacting systems, *Ann. Phys.* **395**, 341 (2018).
- [46] I. Bloch, J. Dalibard, and S. Nascimbene, Quantum simulations with ultracold quantum gases, *Nat. Phys.* **8**, 267 (2012).
- [47] A. P. Orioli, A. Signoles, H. Wildhagen, G. Günter, J. Berges, S. Whitlock, and M. Weidemüller, Relaxation of an isolated dipolar-interacting Rydberg quantum spin system, *Phys. Rev. Lett.* **120**, 063601 (2018).
- [48] T. E. Lee, H. Häffner, and M. Cross, Antiferromagnetic phase transition in a nonequilibrium lattice of Rydberg atoms, *Phys. Rev. A* **84**, 031402 (2011).
- [49] T. Keating, R. L. Cook, A. M. Hankin, Y.-Y. Jau, G. W. Biedermann, and I. H. Deutsch, Robust quantum logic in neutral atoms via adiabatic Rydberg dressing, *Phys. Rev. A* **91**, 012337 (2015).
- [50] L. Buchmann, K. Mølmer, and D. Petrosyan, Creation and transfer of nonclassical states of motion using Rydberg dressing of atoms in a lattice, *Phys. Rev. A* **95**, 013403 (2017).
- [51] A. Mitra, M. J. Martin, G. W. Biedermann, A. M. Marino, P. M. Poggi, and I. H. Deutsch, Robust Mølmer-Sørensen gate for neutral atoms using rapid adiabatic Rydberg dressing, *Phys. Rev. A* **101**, 030301 (2020).
- [52] M. Genkin, S. Wüster, S. Möbius, A. Eisfeld, and J. Rost, Dipole-dipole induced global motion of Rydberg-dressed atom clouds, *J. Phys. B-At. Mol. Opt.* **47**, 095003 (2014).

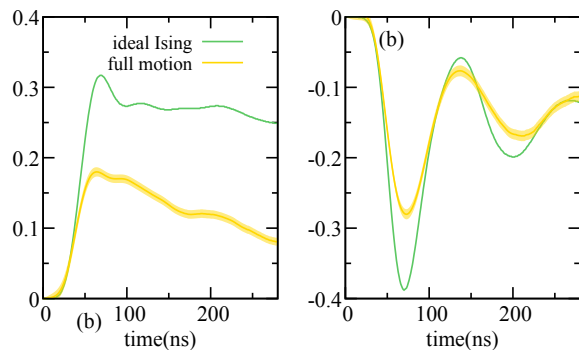


FIG. 6. Nearest-neighbor correlation $C(0,1)$ changes over time (a) off-resonance ($\Delta = -10$ MHz) and (b) at the single-atom resonance ($\Delta = 0$ MHz).

Appendix A: Classical Equation of Motion

According to the Hamiltonian (1), the classical equations of motion are

$$\begin{aligned}
 \dot{r}_i^\alpha &= \frac{p_i^\alpha}{m} \\
 \dot{p}_i^\alpha &= - \sum_{j \in \text{n.n. } i} \frac{3\hbar J a_l^6}{2r_{ij}^8} (r_i^\alpha - r_j^\alpha) (\sigma_i^z + 1) (\sigma_j^z + 1) \\
 &\quad - \frac{\hbar V_0 \pi^2}{a_l^2} \tilde{r}_i^\alpha (1 - \sigma_i^z) \\
 \dot{\sigma}_i^\alpha &= \left[-\frac{\Delta}{2} - \sum_{j \in \text{n.n. } i} \frac{J a_l^6}{2r_{ij}^6} (\sigma_j^z + 1) - \frac{V_0 \pi^2}{2a_l^2} \tilde{r}_i^2 \right] \sum_{\beta} \epsilon^{\alpha\beta z} \sigma_i^\beta \\
 &\quad - \frac{\Omega}{2} \sum_{\beta} \epsilon^{\alpha\beta x} \sigma_i^\beta - \frac{1}{T_1} (-1 + \sigma_i^z) \delta^{\alpha z} - \frac{1}{T_2} \sigma_i^\alpha (1 - \delta^{\alpha z}),
 \end{aligned} \tag{A1}$$

where ϵ^{ijk} is the Levi-Civita symbol, $\delta^{\alpha\beta}$ is the Kronecker delta, and the variables r_i^α , p_i^α , and σ_j^z are c-numbers corresponding to their quantum operator counterparts. The T_1 and T_2 times arise from single particle decoherence. These are the single particle excitation decay time and the dephasing time, respectively.

Appendix B: Dependence of correlations, kinetic energy, and atom number on time

To see how the effect of motion evolves, in Fig. 6 we show the values of the nearest-neighbor correlation $C(0,1)$ over time in the long-time quench at $\Delta = -10$ MHz (far from the single-particle resonance) and

$\Delta = 0$ MHz (on resonance). These roughly are the detunings where atom motion has the largest and smallest effects, respectively. Fig. 6 shows that the effect of motion accumulates over time, as the ideal Ising and full motion curves overlap at the beginning of the quench, but start to show differences after $t = 50$ ns.

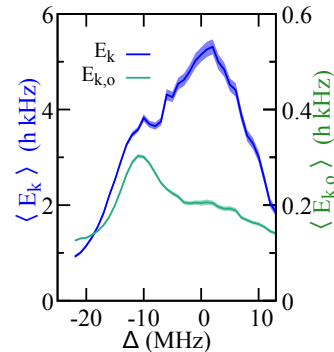


FIG. 7. Average kinetic energy (blue curve) and out-of-plane kinetic energy (green curve) at the end of the long-time quench as a function Δ . Initially, the zero-point energy per direction is $\hbar\omega/2 = h \times 0.108$ kHz.

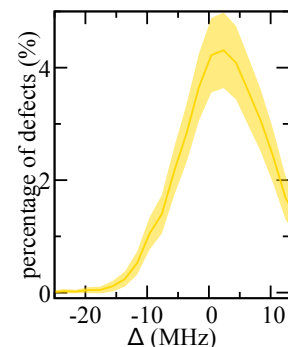


FIG. 8. Percentage of atom loss at the end of the long-time quench as a function of Δ .

To gain insight into the role that atom motion plays in the dynamics, we examine the motional behavior directly. The average kinetic energy in Fig. 7 suggests that, when allowed to move, the kinetic energy of atoms will increase, especially in the in-plane direction. This is consistent with the effects of motional decoherence increasing over time during the quench.

Also, at long enough time some Rydberg atoms will get close enough to each other and react, leading to atom losses. During the dynamics, some atoms can move out of the traps and cause atom loss as well. At the end of dynamics, all lost atoms are treated as Rydberg-state atoms, according to the experimental detection techniques in Ref. [18]. However, as plotted in Fig. 8, after the long-time quench in Sec. III A 2, the fraction of atoms lost by the end of the dynamic is $< 5\%$, a small impact on the simulation results shown.